Different concepts for creating antibacterial yet biocompatible surfaces: adding bactericidal element, grafting therapeutic agent through COOH plasma polymer and their combination

Elizaveta S. Permyakova[1], Anton M. Manakhov[1*], Philipp V. Kiryukhantsev-Korneev[1], Alexander N. Sheveyko[1], Kristina Y. Gudz[1], Andrey M. Kovalskii[1], Josef Polčak[2,3], Irina Y. Zhitnyak[4], Natalia A. Gloushankova[4] , Ivan A. Dyatlov[5] , Sergei G. Ignatov[5,6], Sergey Ershov[7], and Dmitry V. Shtansky[1]

[1] National University of Science and Technology "MISIS", Leninsky prospect 4, Moscow, 119049, Russia
[2] CEITEC—Central European Institute of Technology, Brno University of Technology, Purkyňova 123, Brno, Czech Republic
[3] Institute of Physical Engineering, Brno University of Technology, Technicka 2896/2, 616 69 Brno, Czech Republic
[4] N.N. Blokhin Medical Research Center of Oncology, Kashirskoe shosse 24, Moscow 115478, Russia;
[5] State Research Center for Applied Microbiology and Biotechnology, Obolensk, Moscow Region 142279, Russia
[6] Federal Autonomous Scientific institution "Eastern Center for State Planning" (FANU "Vostokgosplan")
[7] Laboratory for the Physics of Advanced Materials (LPM), Department of Physics and Materials Science, University of Luxembourg, L-1511 Luxembourg

* Correspondence: ant-manahov@ya.ru; Tel.: +7-915-8494059

Abstract

Antibacterial coatings have become a rapidly developing field of research, strongly stimulated by the increasing urgency of identifying alternatives to the traditional administration of antibiotics. Such coatings can be deposited onto implants and other medical devices and prevent the inflammations caused by hospital-acquired infections. Nevertheless, the design of antibacterial yet biocompatible and bioactive surfaces is a challenge that biological community has faced for many years but the "materials of dream" have not yet been developed. In this work, the biocompatible yet antibacterial multi-layered films were prepared by a combination of magnetron sputtering (TiCaPCON film), ion implantation (Ag-doped TiCaPCON film), plasma polymerization (COOH layer), and final immobilization of gentamicin (GM) and heparin (Hepa) molecules. The layer chemistry was thoroughly investigated by means of FTIR and X-ray photoelectron spectroscopies. It was found that the immobilization of therapeutic components occurs throughout the entire thickness of the plasma-deposited COOH layer. The influence of each type of bactericide (Ag^+ ions, GM, and Hepa) on antibacterial activity and cell proliferation was analyzed. Our films were cytocompatible and demonstrated superior bactericidal efficiency toward antibiotic-resistant bacterial *E. coli* K261 strain. Increased toxicity while using the combination of Ag nanoparticles and COOH plasma polymer is discussed.

Introduction

Antibacterial coatings are rapidly emerging as a primary component of the global mitigation strategy of bacterial pathogens, because this is highly efficient approach for prevention of the so-

called nosocomial (hospital-acquired) infections. Such infections are considered as a major health challenge in healthcare units worldwide [1].

There are three major strategies for designing antibacterial coatings based on infection suppression mechanisms: antibacterial agent release, contact-killing, and anti-adhesion/bacteria-repelling [2]. The agent release method is based on the leaching of therapeutic agent (bactericide ions or drugs) leading to the bacterial killing [3]. The contact killing method involves the killing of the bacteria upon their contact with a surface due to the damages induced by specific topography, surface local currents, or charge distributions [4,5] . The anti-adhesion/bacteria-repelling methods are based either on the grafting of anti-adhesion biomolecules or on the modulation of surface superhydrophilicity [2,6].

The main limitations of the existing strategies for the development of antibacterial coatings include (i) the complexity of control of the bactericide agent release, (ii) the relatively short-term antibacterial effect, and (iii) the possible toxicity of bactericidal ions or antibiotics. Obviously, a combination of several strategies modulating the antibacterial effect can be useful due to the synergetic effect of several antibacterial actions. The design of antibacterial yet biocompatible and bioactive surfaces is a challenge that biological community has faced for many years but the "materials of dream" have not yet been developed [7]. Although the bulk properties of materials in healthcare applications have been more or less fully optimized, the implant-related microbial infections remain a serious problem in reconstructive surgery [8]. Surface engineering is an effective tool to impart desirable chemical, biological, and mechanical characteristics to a surface without compromising its bulk properties [9,10]. The modification of chemistry and morphology of an implant surface may significantly affect both antibacterial activity and bioactivity [11–13].

In order to improve the bioactivity of specific materials (e.g. Ti surface in the context of implant devices), a composite Ti-Ca-P-C-O-N film could be very beneficial. As shown earlier, such a layer is highly bioactive [14,15]. In order to endow material with antibacterial effect, the implantation of bactericidal elements (Cu, Ag, etc.) or drug loading were tested [16,17]. However, these approaches only led to a relatively short-term antibacterial effect, whereas longer bacterial protection is required. A long-term controlled release is of high demand in case of complications or reoperation when there is an inflammatory process in the surrounding tissues [18]. Up to date, the design of coatings that can ensure the release of the required level of bactericidal component sufficient to kill bacteria, but safe for eukaryotes, remains a significant challenge.

In the current work, the bioactivity of TiCaPCON surface was further enhanced by deposition of a thin layer of carboxylic plasma polymer using CO_2/C_2H_4 plasma polymerization carried out in the same vacuum chamber in which the TiCaPCON layer was deposited. The deposition experiments were performed at a low-pressure of 2-4 Pa using $Ar/C_2H_4/CO_2$ radio frequency plasma. The resulting TiCaPCON-COOH samples were used as smart platforms for further surface functionalization to impart bactericidal characteristics. The utilization of $Ar/CO_2/C_2H_4$ plasma will provide a stable layer containing carboxylic groups with a good adhesion to the TiCaPCON layer. The COOH groups and the negatively charged surface are expected to provide the growth of hydroxyapatite layer. Moreover, the COOH groups could also serve as active cites for a strong covalent bonding of different active molecules included in the antibiotics [19,20].

The aim of this work is to study the biocompatibility and antibacterial activity of a multicomponent coating system consisting of an Ag-implanted TiCaPCON layer and a top COOH plasma-deposited layer with covalently bonded gentamicin and heparin. Gentamicin was

chosen because it has amino-containing molecules for covalent immobilization with COOH plasma polymer and is widely used for the treatment of bone infections caused by gram-positive and gram-negative bacteria. The bactericide grafting strategy is based on the immobilization of gentamicin by the COOH groups of plasma polymer (deposited on the surface of TiCaPCON layer) *via* the EDC coupling chemistry. Subsequently, the antiadhesive heparin molecules are immobilized on the gentamicin surface through the ionic bonds formed between the positively charged amine groups of gentamicin and the negatively charged COOH groups of heparin.

With such a coating design, gentamicin is covalently bound with the COOH groups of the plasma polymer and the ionically bound with heparin. Due to the different types of chemical bonds, gentamicin is expected to be released rapidly at the beginning of dissolution (due to weaker ionic bonding) and then more slowly (due to stronger covalent bonding). Simultaneously, heparin will provide additional antibacterial effect and stimulate cell viability.

2 Materials and Methods

2.1 Deposition of a TiCaPCON layer and Ag implantation

The deposition experiments were performed using a UVN-2M (Russia) vacuum set-up equipped with magnetron sputtering system, ion source, and MEVVA-type ion implanter. Typical rig scheme is presented in the [21] . The TiCaPCON films were deposited by magnetron sputtering of a composite TiC-CaO-Ti_3PO_x target in a gaseous mixture of Ar and 15% N_2. The applied magnetron current was 2 A, the magnetron voltage was ~ 450 V, and the bias voltage was controlled at -50 V (samples denoted as TiCaPCON throughout the text). The target to substrate distance was fixed to 120 mm. A silver ions were sputtered using an MEVVA-type implanter additional Ar ion source operating with the acceleration voltage of 20 kV and the current of 20 mA (samples hereafter denoted as TiCaPCON-Ag) [22] . The depth of implantation is less than 30 nm and silver tend to form nanodroplets and shallow depth as showed before [5].

2.2 Deposition of a COOH plasma layer

The COOH plasma polymer layer was deposited onto the surface of pristine, TiCaPCON-, and

TiCaPCON-Ag-coated Si wafers. The polymer layer deposition was carried out using second UVN-2M vacuum system equipped with the radio frequency (RF) source. The residual pressure in the vacuum chamber was below 10^{-3} Pa. The plasma was ignited using RF power supply Cito 1310-ACNA-N37A-FF (Comet) connected to the RFPG-128 disk generator (Beams & Plasmas) installed in the vacuum chamber. The pulse period, duty cycle, and the RF power were set to 2.033 μs, 5%, and 500 W, respectively. The operating frequency was 13.56 MHz. CO2 (99.995%), Ar (99.998%), and C2H4 (99.95%) were fed into the vacuum chamber. The gas flow rates were set to 50 (Ar), 16.2 (CO2), and 6.2 (C2H4) sccm and controlled using a Multi Gas Contoller647C (MKS). The pressure in vacuum chamber was measured by VMB-14 unit (Tokamak) and D395-90-000 BOC (Edwards) controllers. The distance between the RF-electrode and the substrate was set to 8 cm. The deposition time was 15 min during which ~100 nm thick plasma coating was formed.

2.3 Gentamicin and heparin loading

Gentamicin (GM) was covalently bonded to the COOH plasma polymer layer by immersion the samples into the 1-Ethyl-3-(3-dimethylaminopropyl) carbodiimide (EDC) (98% Sigma Aldrich) water solution (2 mg/ml) for 15 min, followed by washing with the phosphate buffer saline (PBS), air exposure at room temperature for 120 min, and the final cleaning with de-ionized water. The samples prepared according to this procedure (Fig.1 a,b) hereafter denoted as –COOH-GM.

In order to immobilize heparin, –COOH-GM samples were immersed into 2% heparin water solution for 120 min and then washed with de-ionized water (samples denoted as –COOH-GM-Hepa). The expected bonding is depicted in Fig. 1c. The final GM loading was performed by keeping –COOH-GM-Hepa samples in 2% water solution of GM for 120 min followed by the washing with de-ionized water. The expected bonding is depicted in Fig. 1d. These samples are designated as –COOH-GM-Hepa-GM.

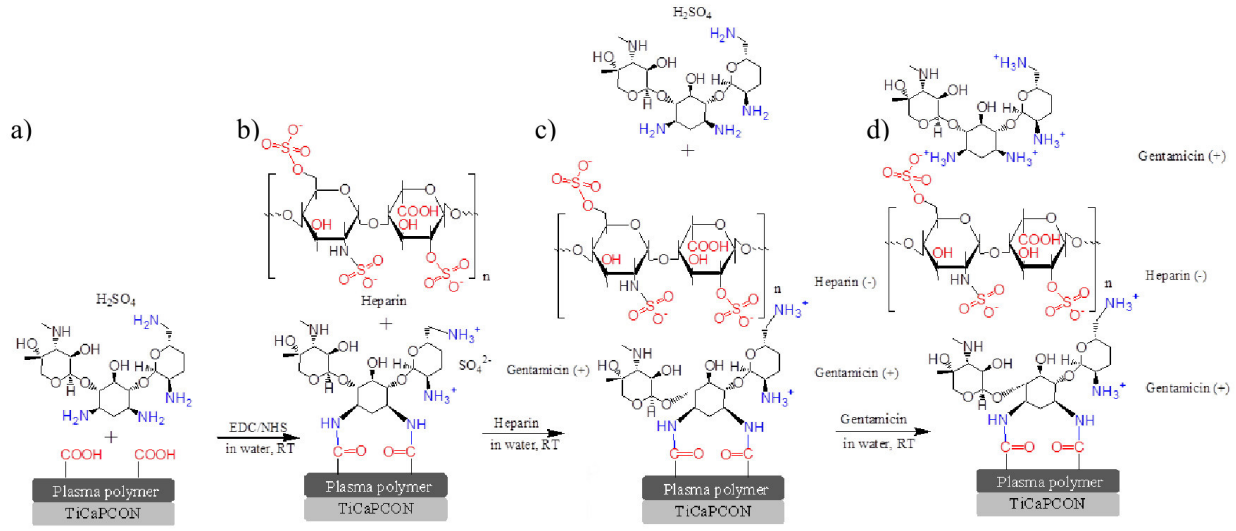

Fig.1 Schematic representation of the GM and heparin immobilization: attachment of GM to the plasma-deposited COOH layer (a), conjugation of heparin with GM-COOH complex (b), attachment of the next GM layer (c), formation of COOH-GM-Hepa-GM multilayer (d).

2.4 Characterization of the layer chemistry and morphology

The TiCaPCON film was investigated using a JSM-7600F Schottky field emission scanning electron microscope (JEOL Ltd.) equipped with an energy-dispersive X-ray (EDX) X-Max 80 Premium detector (Oxford Instruments) operated at 15 kV. To compensate for the surface charging, the samples were coated with a ~5 nm thick Pt layer.
AFM analysis of samples was performed on an Integra Spectra microscope (NT-MDT) using silicon-nitride NSG10 scanning probes (NT-MDT) with a tip radius of 8 ± 2.1 nm.
The chemical composition of surfaces was determined by the X-ray photoelectron spectroscopy (XPS) using an Axis Supra spectrometer (Kratos Analytical). The maximum lateral dimension of the analyzed area was 0.7 mm. The spectra were fitted using the CasaXPS software after subtracting the Shirley-type background. The binding energies (BE) values for all carbon, titanium, and nitrogen environments were taken from the literature [5,19,23]. The BE scale was calibrated by shifting the $\underline{C}H_x$ component to 285.0 eV. XPS depth profiling was performed using

Ar500+ cluster gun with the energy of 10 keV. The size of the crater was 2 by 2 mm. The etching was done in 18 steps (each step was 30s).

2.5 Bactericide release

The concentration of Ag ions released from the sample surfaces into phosphate-buffered saline (PBS, pH 7.4) was studied by inductively coupled plasma mass spectroscopy (ICP-MS) using a X-Series II instrument (Thermo Fisher Scientific). The samples (1 × 1 cm^2) were immersed in flasks filled with 20 mL of PBS and kept at room temperature. Then 1.5 mL aliquots were collected after 1, 3, 8 h and further after 1, 3, 5 and 7 days to analyze the concentration of released ions. The gentamicin/heparin-modified samples with and without Ag were immersed in flasks filled with 20 mL of PBS (pH 7.4) at room temperature. To analyze antibiotic concentration, 500 μL of each supernatant was collected after 1, 3, 8 h and further after 1, 3, 5 and 7 days. After each sampling, the solution volume was increased to the initial one by adding 500 μL of fresh PBS. The antibiotic release kinetics was studied by means of an UV spectrophotometer (Ocean Optics). Measurements were performed in the wavelength range of 0−1000 nm. The maximum absorption intensities for gentamicin and heparin were 224 and 256 nm, respectively, which were used for further quantification. Curve of samples containing both therapeutic agents were fitted by Multiple Peak Fit Tool (Origin Pro 2018). To plot a calibration curve, absorbance of antibiotic solutions with concentrations in the range of 0.005−4 mg/ mL was measured. The antibiotic concentration released into PBS over time was evaluated by comparing with the calibration curve. Experiments on the drug release were carried out in triplicate for each antibiotic type.

2.6 Analysis of osteblastic cell proliferation

MC3T3-E1 cells (10^4 cells/ml) were seeded on the surface of samples placed into 12-well plates containing 2 ml of DMEM/F12 culture medium per well (a 1:1 mixture of Dulbecco's Modified Essential Medium (DMEM) and Ham's F-12 Medium) (Gibco) with 10% of fetal calf serum (PAA). The cultures were grown in a humidified atmosphere with 5% of CO2 at 37 ^oC for 24 h. After 1, 3, 5, and 7 days of incubation, cells were fixed with 3.7% paraformaldehyde and stained with 4′,6-Diamidine-2′-phenylindole dihydrochloride (DAPI) (Sigma). The number of cells in the field was determined with an Zeiss Axioplan microscope (Zeiss, Germany) equipped with a ×40 objective. The mean values of thirty examined fields for each tested plate were calculated. All data reported as MEAN ± SEM. The statistics was analyzed according to Kruskal-Wallis criteria.

2.7 Antibacterial activity

The antibacterial activity of samples was evaluated against clinically isolated antibiotic-resistant bacterial *E. coli* K261 strain. The bacterial cells were cultivated either in Luria-Bertani (LB) broth medium or onto solid LB-agar. The LB-broth medium consisted of 10 g of bacto-trypton, 5 g of yeast extract, and 5 g of NaCl in 1 L of distilled water. The LB-agar contained LB-broth medium (prepared as described above) and 18 g of agar in 1 L of distilled water. For quantitative evaluation, the samples were placed in the sterile 12-well culture plate (Corning Costar) with 0.5 mL of normal saline solution (0.9% saline, hereafter denoted as NSS) and incubated in a thermostat at 37 °C. Then, 0.03 mL of overnight bacterial culture was added to the plates in such a way that the tested samples were fully immersed in the bacterial suspension. One sample-free well was used as a control. After 3 and 24 h, the concentration of bacterial colony forming units (CFUs) was determined by decimal dilution in 0.3 mL of NSS. One hundred μL of decimal

diluted suspension was dispersed onto a solid nutrient agar in sterile Petri dishes. The number of surviving CFUs in each Petri dish was counted after incubation at 37°C for 3 and 24 h. The values of CFUs for three Petri dishes with the same samples were averaged.

3 Results and discussion

3.1 Morphology of deposited films.

Figure 2 compares the surface morphologies of Si-(TiCaPCON)-COOH, Si-(TiCaPCON)-COOH-GM, Si-(TiCaPCON)-COOH-GM-Hepa, and Si-(TiCaPCON)-COOH-GM-Hepa-GM samples. Without a polymer layer, the TiCaPCON surface is covered with 3D islands with lateral size in the range of 15-35 nm (Fig. 2a). After GM deposition, the cauliflower-like homogenous surface morphology has not changed (Fig. 2b). Heparin immobilization led to the appearance of smaller surface topographical features, apparently as a result of a new nucleation and growth (Fig. 2c). Grafting of the second layer of gentamicin led to the disappearance of small surface features; an average lateral size of 3D surface hills was approximately 50 nm (Fig. 2d). The morphology of our samples was also confirmed by AFM measurements (see the Supporting Inormation)

3.2 Elemental compositions of TiCaPCON and TiCaPCON-Ag layers

The elemental compositions of the TiCaPCON and TiCaPCON-Ag layers, as determined by XPS analysis, are given in Table 1. After Ag^+ ion implantation, in addition to the presence of Ag (~2 at.%), the titanium and oxygen concentrations were observed to significantly increase at the expense of carbon and nitrogen.

Table 1 Sample elemental compositions as derived from the XPS analysis.

	Concentration, at.%						
Sample	Ti	C	O	N	Ag	Ca	S
Si-TiCaPCON	9.7	58.4	22.0	8.7	0.0	1.3	0.0
Si-TiCaPCON-Ag	14.0	37.4	42.5	3.1	2.0	1.0	0.0
Si-TiCaPCON-COOH	0.0	77.9	22.1	0.0	0.0	0.0	0.0
Si-TiCaPCON-Ag-COOH	0.0	72.4	23.5	3.6	0.5	0.0	0.0
Si-TiCaPCON-(Ag)-COOH-GM	0.0	75.1	19.6	5.0	0.0	0.0	0.3
Si-TiCaPCON-(Ag)-COOH-GM-Hepa	0.0	74.4	19.7	5.4	0.0	0.0	0.5
Si-TiCaPCON-(Ag)-COOH-GM-Hepa-GM	0.0	70.4	23.3	5.8	0.0	0.0	0.5

In order to thoroughly analyze the functional composition of the TiCaPCON and TiCaPCON-Ag surfaces, the C1s, Ti2p, and N1s signals were fitted using CasaXPS software (Fig. 3).

The XPS Ti2p signal of the TiCaPCON layer is shown in Fig. 3a. Due to the better-resolved Ti 2p 3/2 signal as compared to Ti 2p ½ counterpart, the first peak was used for further XPS analysis. The XPS Ti2p 3/2 peak was fitted using three components (Fig. 3a): TiC (BE=455.3 eV, FWHM=1.2 eV), TiN (BE=456.6 eV FWHM=1.8 eV), and TiO_2 (BE=458.5 eV, FWHM=1.6 eV), indicating the presence of carbide, nitride, and oxide states on the TiCaPCON surface. The fitting of C1s and N1s spectra also confirmed the presence of nitride and carbide

(Fig 3b,c). The C1s peak was fitted by the sum of four components: hydrocarbons titanium carbide Ti-C (BE=282.5 eV), hydrocarbons CH_x (BE=285 eV), ether C-O group (BE=286.5 eV), and carbon doubly bonded to oxygen C=O (BE=288.0 eV). For all four components, the full width at the half maximum (FWHM) was set to 1.6±0.1 eV. The N1s signal was fitted with a sum of three components: Ti-N (BE=397.1 eV), C-N (BE=399.2 eV), and NH_3^+ (BE=401.2 eV).

The XPS spectra of the TiCaPCON-Ag layer were significantly different. First, the Ti2p signal revealed only one type of the environment, i.e. titanium dioxide (Fig. 3d). The absence of titanium carbide was also supported by the C1s curve fitting (Fig. 3e). In addition, the N1s signal showed no nitride peak (see Supporting Information, Figure S1). A single asymmetric Ag 3d 5/2 maximum centered at 368.2 eV indicated that Ag is in a metallic state (Fig. 3i).

The deposition of COOH plasma layer on both the TiCaPCON and TiCaPCON-Ag films resulted in very similar surfaces. However, certain differences between the XPS spectra of TiCaPCON-COOH (Fig. 4a) and TiCaPCON-Ag-COOH samples (Fig. 3h) can be noted. Although for both surfaces no Ti was observed (the XPS wide scan of this sample presented in Supporting Information, Fig. S2), the TiCaPCON-Ag-COOH sample displays a XPS Ag3d peak (0.5 at.%) indicating that not all Ag nanoparticles are covered by the COOH plasma layer. The Ag state remained the same as for the TiCaPCON-Ag sample, i.e. metallic nature (Fig. 3i). Thus, in addition to the active COOH groups designed for covalent attachment of a therapeutic agent, the presence of silver on the TiCaPCON-Ag-COOH surface offers an additional advantage in terms of antibacterial properties.

Furthermore, the TiCaPCON-Ag-COOH film contained small amount of nitrogen (3.6 at.%) on its surface. The N1s signal analysis (see Fig. S1, Supporting information) revealed that nitrogen is in the amide environment (N-C=O). Note, however, that as follows from Fig. 3g,h, carbon to oxygen bonds form the basis of COOH layer.

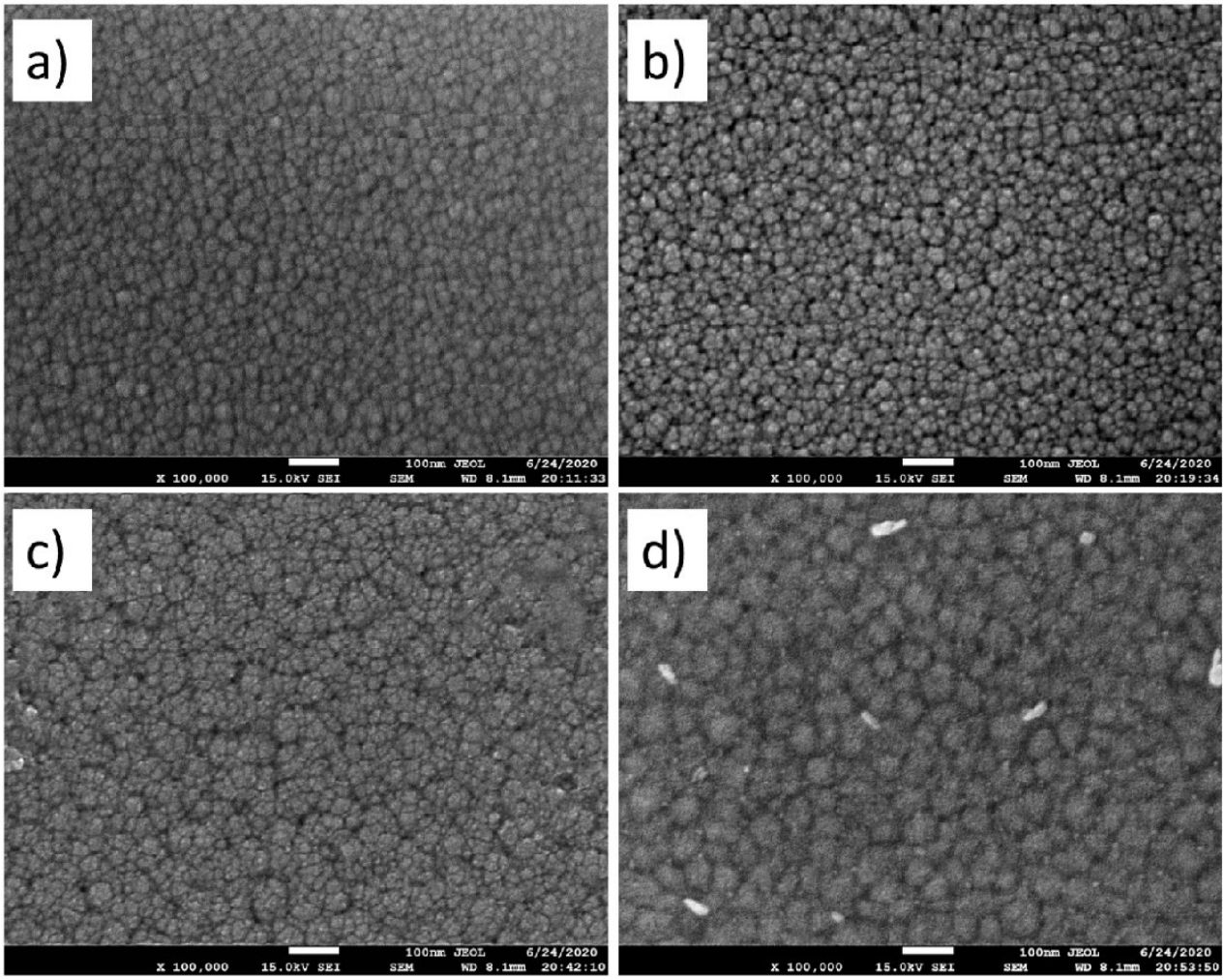

Fig. 2 SEM images of Si-TiCaPCON-COOH (a), Si-TiCaPCON-COOH-GM (b), Si-TiCaPCON-COOH-GM-Hepa (c), and Si-TiCaPCON-COOH-GM-Hepa-GM (d) samples.

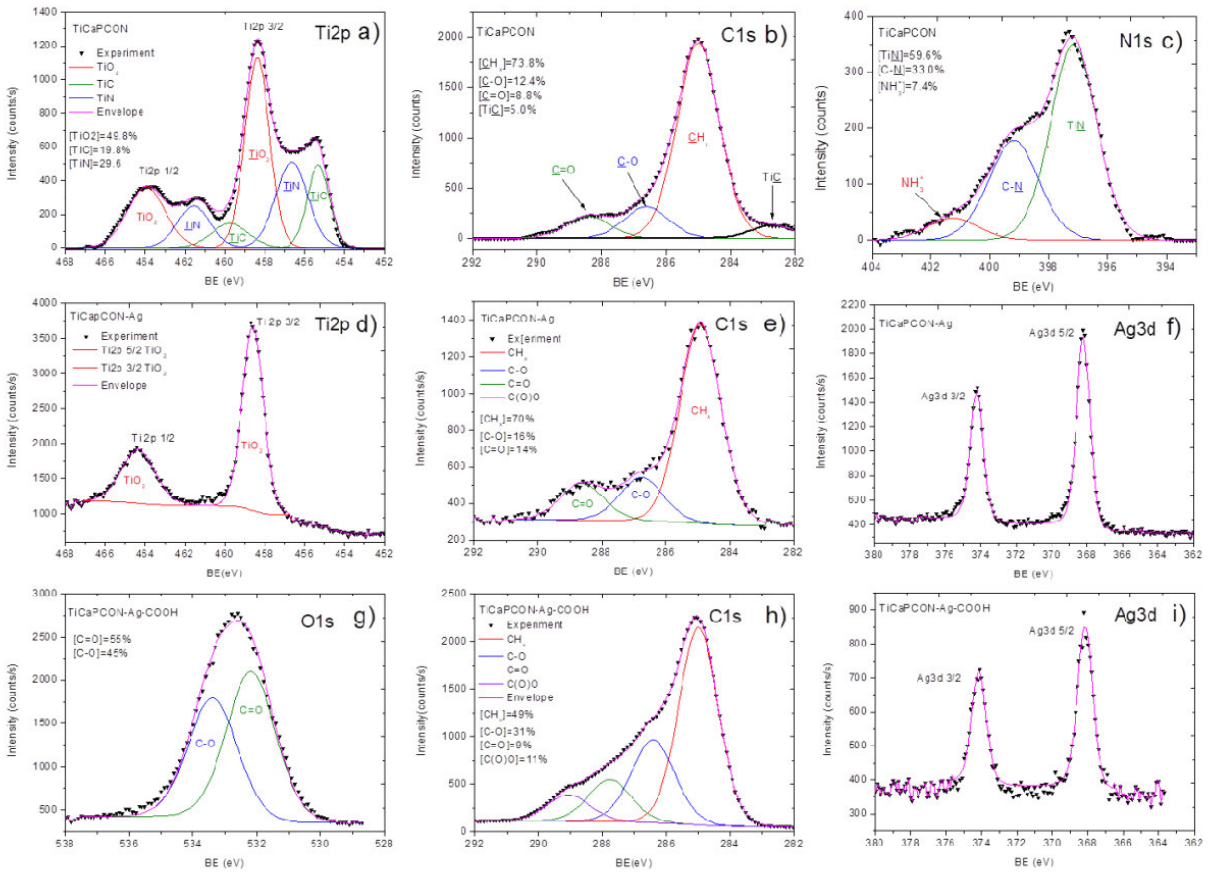

Fig.3 XPS spectra and their curve fitting for TiCaPCON (a-c), TiCaPCON-Ag (d-f), and TiCaPCON-Ag-COOH films (g-i). Ti2p (a,d), C1s (b,e,h), N1s (c), Ag3d (f,i) and O1s (g).

3.3 Gentamicin and heparin immobilization

The immobilization of GM, heparin as well as the final loading of GM on the top of heparin layer led to minor changes of the TiCaPCON-COOH morphology (Fig 2 b,c,d). It was observed that the size of agglomerates became larger after each successive treatment step, this being particularly noticeable after the final step (TiCaPCON-COOH-GM-Hepa-GM).

As noted above, the surface sensitive XPS technique reveals little difference in surface chemistry of the TiCaPCON-COOH and (TiCaPCON-Ag)-COOH samples. After therapeutic agent immobilization, no difference in surface composition between the Ag-doped and Ag-free samples was observed. Therefore, the XPS results only for Ag-implanted samples after gentamicin and heparin immobilization are presented below. For FT-IR spectroscopy analysis, a simple Si-COOH system, both before and after GM and Hepa immobilization was used.

The C1s signals of the TiCaPCON-COOH, (TiCaPCON-Ag)-COOH-GM, (TiCaPCON-Ag)-COOH-GM-Hepa, and (TiCaPCON-Ag)-COOH-GM-Hepa-GM samples were fitted with a sum of four peaks: CH_x (BE=285.0 eV), **C**-N/C-O (BE=286.4±0.1 eV eV), C=O/N-C=O (BE=288.0±0.1 eV), and C(O)O (BE=289.1 ±0.05 eV eV). The FWHM value for all components was set to 1.6±0.15 eV. As can be seen in Fig 4 (left column), the difference in carbon environment between four samples is very small. In contrast, nitrogen signal can be used as a fingerprint of the successful GM immobilization. As shown in Table 1 and Fig. 4 (right column), no nitrogen was determined before the GM immobilization, whereas the TiCaPCON-COOH-GM surface exhibited [N]=5.0 at.%. The XPS N1s peak was fitted with the sum of two well-known

components: the amide environement (N-C=O, BE=399.9 eV) and the protonated amines (NH_3^+, BE=401.4 eV. The formation of the amide bonds (N-C=O) is also consistent with the appearance of peak around 1626 cm^{-1} in the corresponding FT-IR spectrum of the Si-COOH-GM sample (Fig. 5). Thus, both the XPS and FT-IR spectroscopy results confirm the successful immobilization of GM on the TiCaPCON-COOH surface (Fig. 1a).

The successful immobilization of heparin is supported by a small increase in the sulfur content (in the sulfate form) on the sample surface as well as by a change in nitrogen environment, namely by a decrease of the protonated amines component (Fig. 4f). FT-IR analysis also revealed significant changes in the surface chemistry of the Si-COOH-GM-Hepa sample as compared to its Hepa-free counterpart (Si-COOH-GM). The intensity of CH_2 (~1450 cm^{-1}) and SO_4^{2-} (1045 cm^{-1}) peaks increased and an additional N-H bending peak of the amide bond (1575 cm^{-1}) appeared. Thus, compared with previous studies [24], our results are more convincing evidence of the attachment of heparin to the active sites of gentamicin.

The loading of GM into the TiCaPCON-COOH-GM-Hepa film led to further changes in the N1s spectrum such as the appearance of a new component corresponding to the non-protonated amines (curve fitting in Fig. 4h). The FT-IR analysis of the Si-COOH-GM-Hepa-GM sample revealed a minor increase in the intensity of the N-H bending and C-N stretching peaks suggesting that only a small amount of GM was grafted. Indeed, the ionic bonding of positively charged gentamicin onto negatively charged heparin is significantly less efficient compared to the covalent bonding of gentamicin onto COOH groups, because ionic bonding is weaker and led to lower density of grafted GM molecules. As a result, the additional loading with GM occurs only at the top heparin surface and thus is only detected by surface sensitive XPS analysis.

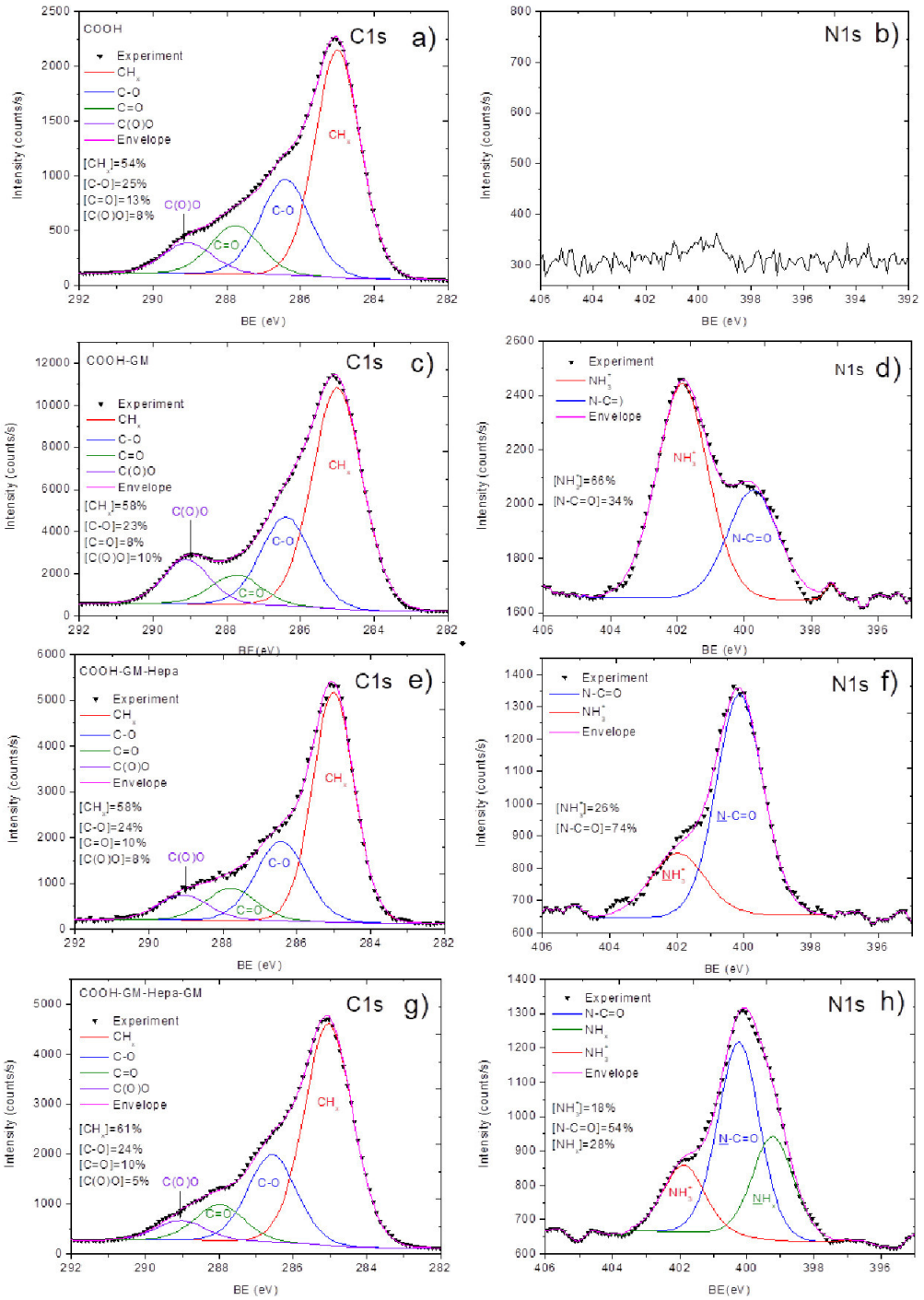

Fig.4 XPS spectra and their curve-fitting for COOH- (a,b), COOH-GM- (c,d), COOH-GM-Hepa- (e,f), and COOH-GM-Hepa-GM-functionalized surfaces. C1s (a,c,e,g) and N1s (b,d,f,h).

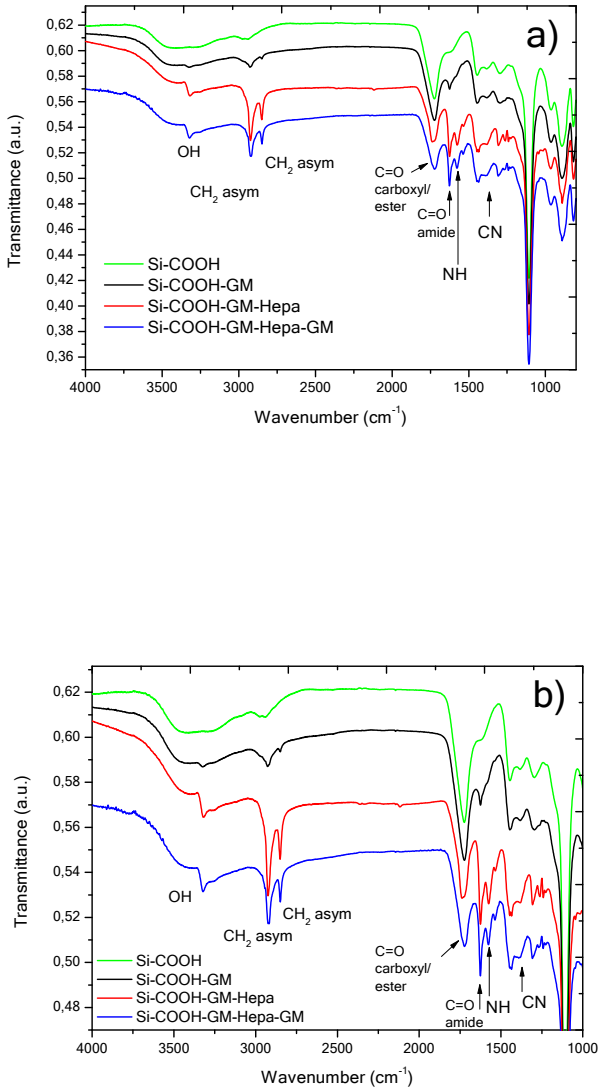

Fig.5 Full-range FT-IR spectra of the Si-COOH, Si-COOH-GM, Si-COOH-GM-Hepa, and Si-COOH-Hepa-GM samples (a) and their zoomed view in the range of 2000 - 900 cm^{-1} (b).

3.4 Depth profile of Si-COOH-GM-Hepa-GM film

Thickness of the immobilized therapeutic agent to the COOH plasma polymer is important for practical medical applications. Depending on the reaction depth, the drug loading capacity and the kinetics of its release can be different. For example, if immobilization only occurs to the topmost COOH layer an increase in polymer thickness will not increase the drug loading capacity. In contrast, if immobilization reaction proceeds over entire depth of the COOH layer, then by adjusting the polymer layer thickness, it will be possible to control the antibacterial agent leaching.

The XPS element depth profiles of Si-COOH-GM-Hepa-GM sample are shown in Fig 6a. Sulfur and nitrogen are distributed inside the entire COOH layer and the content of both elements

significantly decreases near the Si wafer surface. The distribution of nitrogen and sulfur is neither stochastic nor affected by the surface roughness. Note that carbon and oxygen concentrations are quite stable over the entire COOH layer depth.

By looking closely at carbon components (Fig. 6b), it becomes clear that there is a correlation between the C-O/C-N ratio and CH_x content: while the nitrogen content in the film decreases, the CH_x component increases. The depth profile analysis (Fig. 6c) of the XPS N1s spectra also shows that the amount of N-containing components decreases with polymer depth. Summarizing all the XPS profiling data, it can be concluded that both gentamicin and heparin are present inside the COOH layer and their concentrations decrease with polymer layer depth.

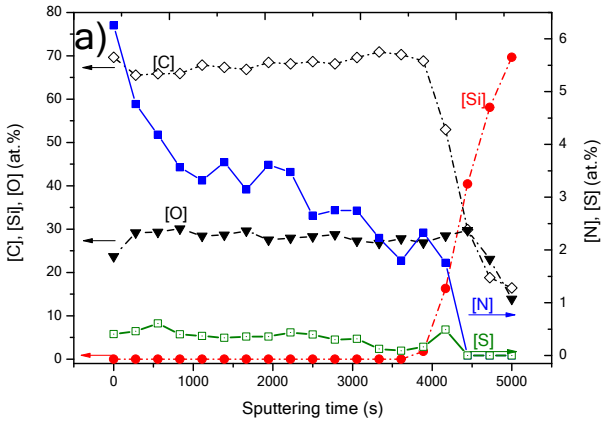

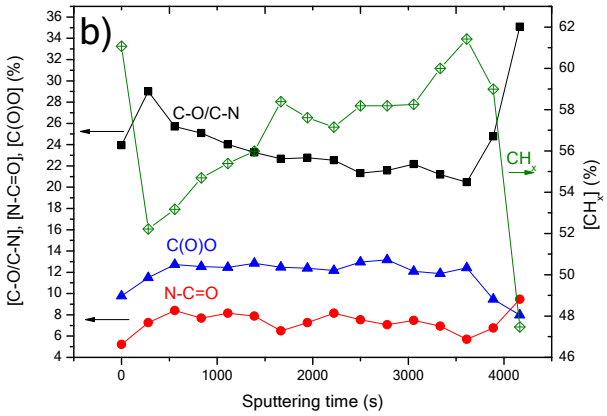

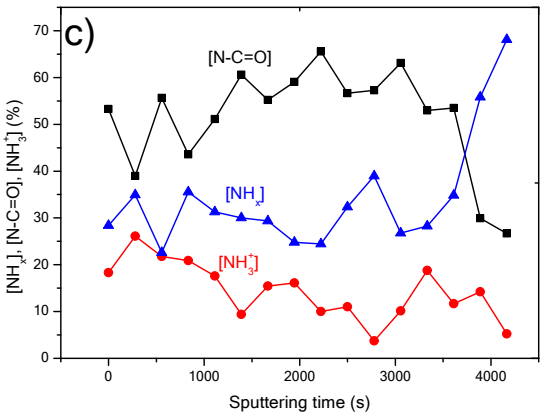

Fig. 6. XPS depth profiles of the Si-COOH-GM-Hepa-GM sample. Atomic compositions (a), carbon (b) and nitrogen (c) environments.

3.5 Bactericide release

Figure 7 shows the concentrations of Ag^+ ions, gentamicin, and heparin released from different samples in PBS *versus* time. In the case of TiCaPCON-Ag film, the concentration of Ag^+ ions rapidly increased to 210 ppb within 12 h and then the release of ions slowed down and almost completely stopped after 120 h (Fig. 7a). The presence of additional surface layers (COOH, GM, heparin, and their combinations) retarded Ag^+ ion leaching: the thicker the layer, the lower the ion concentration. Gentamicin can interact with Ag^+ ions to form stable Ag/gentamicin complexes, hereby depleting the concentration of bactericide ions in solution [24]. However, as follows from a comparison of ion release for the TiCaPCON-Ag-COOH and TiCaPCON-Ag-GM samples, if such an interaction occurs, it does not significantly affect the Ag^+ ion concentration.

An intensive gentamicin release during 24 h was followed by a slower antibiotic leaching (Fig. 7b). The gentamicin concentration depended on the loading doze (one or two antibiotic layers) and after 24 h varied from 100 μg/mL (TiCaPCON-Ag) to 275 μg/mL (TiCaPCON-Ag-GM-Hepa-GM). Interestingly, the presence of Ag accelerated gentamicin leaching. This may be due to the capture of gentamicin species during intensive Ag^+ ion release. Note that both the accelerated [25,26] and delayed [21] gentamicin release in the presence of silver ions was reported. Almost all heparin released within 24 h. The existence of top GM layer slightly retarded heparin leaching (Fig. 7c).

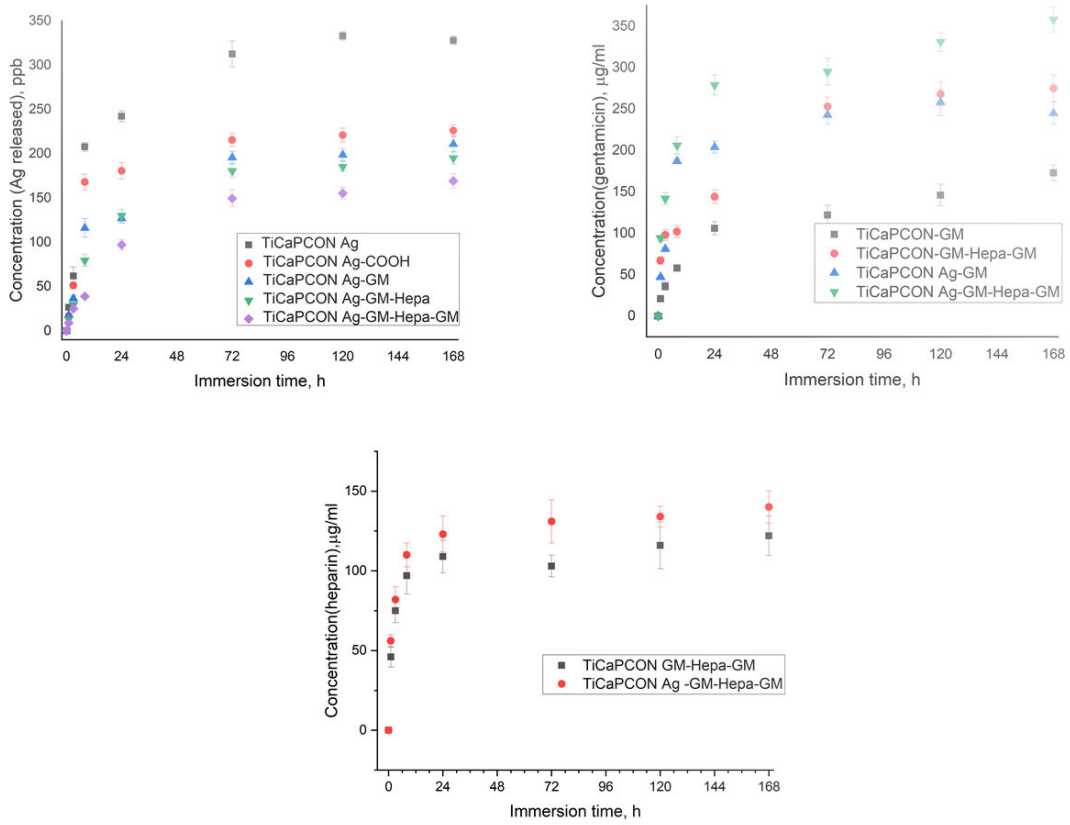

Fig. 7. Concentration of Ag^+ ions (a) and an amount of gentamicin (b) and heparin (c) released in a PBS *versus* time.

3.6 Cell proliferation study

The cytocompatibility of all samples were evaluated using the cell proliferation rate analysis (Fig. 8). Similar to the control (glass and TiCaPCON), the TiCaPCON-Ag and TiCaPCON-COOH-GM-Hepa samples exhibited a high rate of osteoblastic proliferation indicating their biocompatibility. Thus Ag^+ ions released from the TiCaPCON-Ag film did not affect the dynamic of bone cell proliferation. The TiCaPCON-COOH sample also demonstrated a positive dynamics in cell proliferation, albeit slightly delayed relative to control (at day 3). This can be explained by releasing of carboxylic acid-containing moieties that can induce toxicity [27]. The TiCaPCON-Ag-COOH-GM and TiCaPCON-COOH-GM samples were also able to maintain a relatively high level of osteoblastic cell proliferation, even higher compared to TiCaPCON-COOH. TiCaPCON-COOH-GM-Hepa and TiCaPCON-Ag-COOH-GM-Hepa films showed also very good cell proliferation rates. Only TiCaPCON-Ag-COOH film exhibited very bad results (no cell proliferation) due to delamination of the layer during the test (the testing was repeated three times) and, hence, TiCaPCON-Ag-COOH was toxic for cells, although we confirmed good stability of TiCaPCON-Ag-COOh in water (see Supporting Information) Most probably the delamination in this particular case related to the presense of Ag nanoparticles with the size of > 100 nm that decreased the mechanical stability of multilayer samples.Interestingly, the subsequent samples prepared within the same batch (TiCaPCON-Ag-COOH-GM, TiCaPCON-Ag-COOH-GM-Hepa, etc.) exhibited very good biocompatibility. Such interesting behavior can be related to the corssliking effect that is achieved thanks to the reaction between multiple amine groups from GM and COOH groups in the coating. Indeed, as GM molecules were penetrating inside the layer, such crosslinking anchor the samples TiCaPCON-Ag_COOH-GM and following ones.

The comparison of cell proliferation and bactericide release tests indicates that the concentration of Ag^+ ions in the range of 300-330 ppb (TiCaPCON-Ag sample) did not affect significantly the dynamics of osteoblastic cell proliferation, being in a good agreement with previous results [21]. Despite the high concentrations of therapeutic agents (100-120 μg/mL for heparin and 250-270 μg/mL for gentamicin), which was reached during immersing the gentamicin and heparin containing films in PBS, the Ag-free samples were able to maintain high proliferation rate of osteoblastic cells. In contrast, materials that simultaneously release Ag^+ ions and gentamicin may exhibit increased cytotoxicity [28]. This can be well illustrated with the TiCaPCON-Ag-COOH-GM sample. Due to extensive Ag^+ ions and gentamicin leaching within 72 h (Fig. 7a,b), no osteoblastic cell proliferation was observed (Fig. 8). However, after 3 days, when the release of ions and antibiotics almost completely stopped, the number of cells increased sharply.

It is worth to noting, that the combination of Ag nanoparticles and COOH plasma polymer led to increased toxicity. One possible explanation for this could be the synergistic effect of Ag^+ ions and carboxylic acid-containing moieties. Another factor that should be taken into consideration is the simultaneous release of Ag^+ ions and carboxylic acid -COOH groups, which can result in increased level of reactive oxygen species (ROS). The reaction of Ag^+ ions with molecular oxygen under aerobic conditions generates superoxide radicals and other ROS [29]. The released carboxylic acid moieties can undergo oxidation into a pro-oxidant species [30]. Overproduction of ROS can induce oxidative stress, resulting in cells failing to maintain normal physiological redox-regulated functions [31] though damaging proteins, nucleic acids, and DNA, cell signaling, and weakening cell antioxidant defense capacity [32-35]. Finally, Ag^+ ions may induce faster layer degradation due to several possible processes: faster degradation induced by ROS and/or faster layer dissolution due to formation of soluble complexes between Ag+ and COOH groups of the plasma layer (some organic acid salts of silver are quite soluble).

a)

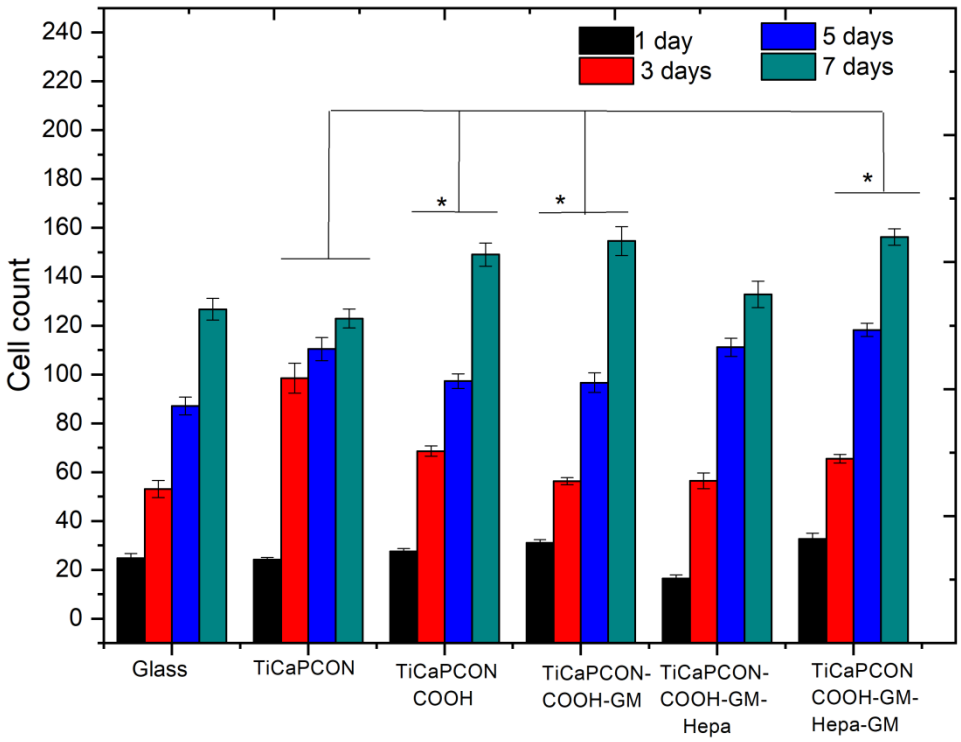
1 day
3 days
5 days
7 days
Cell count
0
20
40
60
80
100
120
140
160
180
200
220
240
*
*
*
Glass
TiCaPCON
TiCaPCON COOH
TiCaPCON-COOH-GM
TiCaPCON-COOH-GM-Hepa
TiCaPCON COOH-GM-Hepa-GM

b)

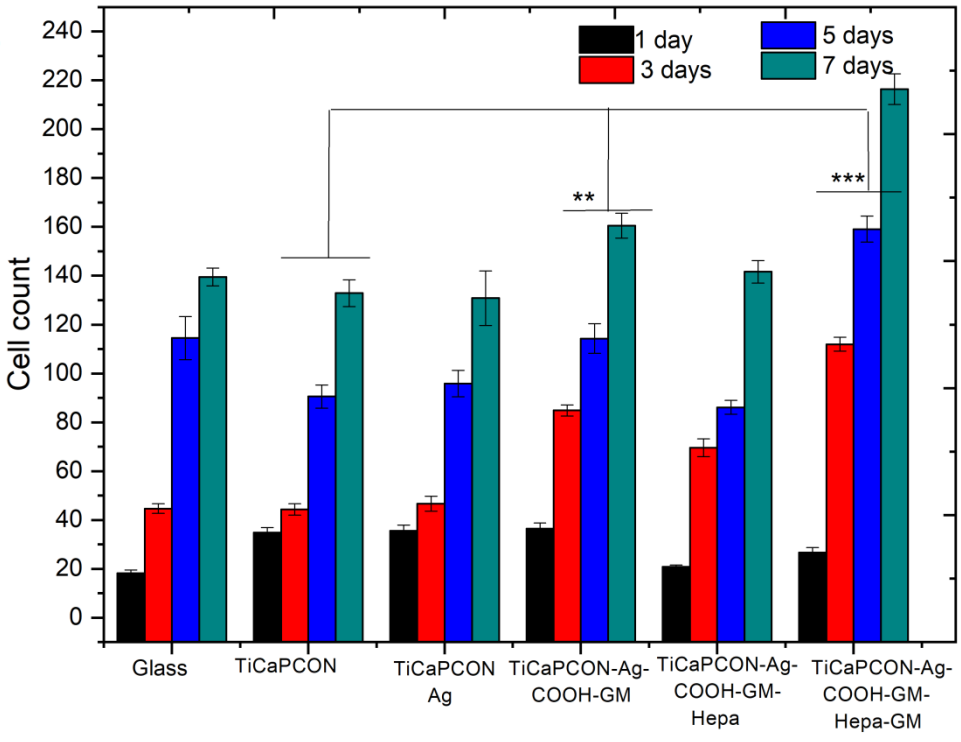
1 day
3 days
5 days
7 days
Cell count
0
20
40
60
80
100
120
140
160
180
200
220
240
**
***
Glass
TiCaPCON
TiCaPCON Ag
TiCaPCON-Ag-COOH-GM
TiCaPCON-Ag-COOH-GM-Hepa
TiCaPCON-Ag-COOH-GM-Hepa-GM

Fig. 8. Osteoblastic cell proliferation on the surface of tested samples without Ag implantation (a) and with Ag implantation. The statically significance was calculated according to Kruskal-Wallis criteria: * $p<0.01$, ** $p<0.001$, *** $p<0.0001$.

3.7 *Antibacterial activity*

The bactericidal activity of samples against antibiotic-resistant bacterial *E. coli* K261 strain is shown in Fig. 9. Already after 3 h of incubation, all samples revealed a noticeable antibacterial effect: 35% (TiCaPCON-Ag), 50% (TiCaPCON-Ag-COOH, TiCaPCON-Ag-COOH-GM, and TiCaPCON-Ag-COOH-GM-Heap-Gm), 70% (TiCaPCON-COOH and TiCaPCON-COOH-GM-Hepa), and 90% (TiCaPCON-COOH-GM). After 24 h, all bacterial cells were inactivated on the surface of TiCaPCON-COOH-GM, TiCaPCON-COOH-GM-Hepa, TiCaPCON-Ag-COOH, TiCaPCON-Ag-COOH-GM, and TiCaPCON-Ag-COOH-GM-Hepa-GM films. For TiCaPCON-Ag sample, the bacteria-killing rate was slower, although, after 24 h, 4-log reduction in the CFU/ml was observed.

The obtained results indicate that two samples, TiCaPCON-Ag and TiCaPCON-COOH-GM-Hepa, are cytocompatible and show high bactericidal efficiency toward antibiotic-resistant bacterial *E. coli* K261 strain. Thus, we demonstrated successful feasibility of two concepts: adding bactericidal element and grafting therapeutic agent through COOH plasma polymer. In contrast, the combination of bactericidal Ag^+ ions and therapeutic agents did not lead to noticeable synergistic antibacterial effect, but retard osteoblastic cell growth.

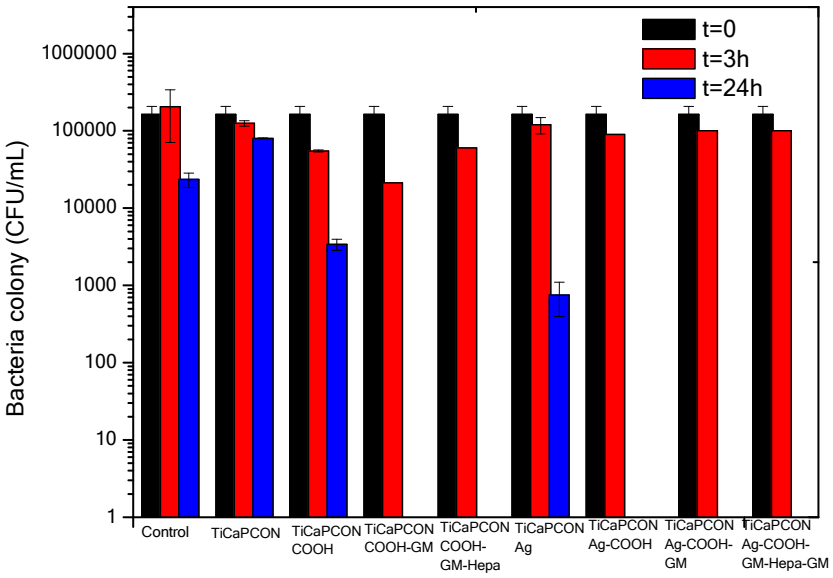

Fig. 9. Antibacterial activity of samples against E. coli K-261 strain.

Conclusions

1) In this work we showed different concepts for creating antibacterial yet biocompatible surfaces, namely adding bactericidal element (Ag) and grafting therapeutic agents through COOH plasma polymer to TiCaPCON film. In addition, two types of gentamicin linkage were considered: the covalent bonding to the COOH groups of plasma polymer and the ionic bonding to heparin.
2) The successful immobilization of gentamicin and heparin to the plasma-deposited COOH layer was confirmed by FTIR and XPS spectroscopies. Both therapeutic agents were present inside the COOH layer and their concentrations decreased with polymer layer depth.
3) During exposure in phosphate-buffered saline, the samples demonstrated a fast release of Ag^+ ions, gentamicin, and heparin within the first 24 h, after which the leaching of heparin stoped, whereas Ag^+ ions and gentamicin released for 120 h. The presence of Ag accelerated gentamicin leaching.
4) The TiCaPCON-Ag and TiCaPCON-COOH-GM-Hepa films were cytocompatible and demonstrated superior bactericidal efficiency toward antibiotic-resistant *E. coli* K261 strain. The TiCaPCON-COOH and TiCaPCON-Ag-COOH-GM films were also able to maintain a relatively high level of osteoblastic cell proliferation and significantly reduced a number of bacterial colony units (more than 1- and 2-log reduction in the CFU/ml after 24 h, respectively). The surfaces of TiCaPCON-Ag-COOH and TiCaPCON-Ag-COOH-GM-Hepa films were toxic for osteoblastic cells.

Acknowledgments

The work was supported by the the Ministry of Education and Science of the Russian Federation in the frame of the Increase Competitiveness Program of NUST "MISiS" (Agreement No. K2-2020-004). J.P gratefully acknowledges CzechNanoLab Research Infrastructure supported by MEYS CR (LM2018110).

References

1. McFee, R.B. Nosocomial or Hospital-acquired Infections: An Overview. *Disease-a-Month* **2009**, *55*, 422–438.

2. Cloutier, M.; Mantovani, D.; Rosei, F. Antibacterial Coatings: Challenges, Perspectives, and Opportunities. *Trends Biotechnol.* **2015**, *33*, 637–652.

3. de Avila, E.D.; Castro, A.G.B.; Tagit, O.; Krom, B.P.; Löwik, D.; van Well, A.A.; Bannenberg, L.J.; Vergani, C.E.; van den Beucken, J.J.J.P. Anti-bacterial efficacy via drug-delivery system from layer-by-layer coating for percutaneous dental implant components. *Appl. Surf. Sci.* **2019**, *488*, 194–204.

4. Ponomarev, V.A.; Sheveyko, A.N.; Sukhorukova, I.V.; Shvindina, N.V.; Manakhov, A.M.; Zhitnyak, I.Y.; Gloushankova, N.A.; Fursova, N.K.; Ignatov, S.G.; Permyakova, E.S.; et al. Microstructure, chemical and biological performance of boron-modified TiCaPCON films. *Appl. Surf. Sci.* **2019**, *465*.

5. Ponomarev, V.A.; Sukhorukova, I. V; Sheveyko, A.N.; Permyakova, E.S.; Manakhov, A.M.; Ignatov, S.G.; Gloushankova, N.A.; Zhitnyak, I.Y.; Lebedev, O.I.; Polčak, J.; et al. Antibacterial Performance of TiCaPCON Films Incorporated with Ag, Pt, and Zn: Bactericidal Ions Versus Surface Microgalvanic Interactions. *ACS Appl. Mater. Interfaces* **2018**, *10*, 24406–24420.

6. Kolewe, K.W.; Dobosz, K.M.; Rieger, K.A.; Chang, C.C.; Emrick, T.; Schiffman, J.D. Antifouling Electrospun Nanofiber Mats Functionalized with Polymer Zwitterions. *ACS Appl. Mater. Interfaces* **2016**, *8*, 27585–27593.

7. Sukhorukova, I. V; Sheveyko, A.N.; Kiryukhantsev-korneev, P. V; Zhitnyak, I.Y. Toward bioactive yet antibacterial surfaces. *Colloids Surfaces B Biointerfaces* **2015**, *135*, 158–165.

8. Doble, M.; Kumar, T.S.; Kiran, A.; Ramakrishna, S.; Sanghavi, R. Antibacterial and Bioactive Surface Modifications of Titanium Implants by PCL/TiO2 Nanocomposite Coatings. *Nanomaterials* **2018**, *8*, 860.

9. Jin, Y.; Zhu, Z.; Liang, L.; Lan, K.; Zheng, Q.; Wang, Y.; Guo, Y.; Zhu, K.; Mehmood, R.; Wang, B. A facile heparin/carboxymethyl chitosan coating mediated by polydopamine on implants for hemocompatibility and antibacterial properties. *Appl. Surf. Sci.* **2020**, *528*, 146539.

10. Zheng, Y.; Miao, J.; Zhang, F.; Cai, C.; Koh, A.; Simmons, T.J.; Mousa, S.A.; Linhardt, R.J. Surface modification of a polyethylene film for anticoagulant and antimicrobial catheter. *React. Funct. Polym.* **2016**, *100*, 142–150.

11. Bazaka, O.; Bazaka, K.; Truong, V.K.; Levchenko, I.; Jacob, M. V; Estrin, Y.; Lapovok, R.; Chichkov, B.; Fadeeva, E.; Kingshott, P.; et al. Effect of titanium surface topography on plasma deposition of antibacterial polymer coatings. *Appl. Surf. Sci.* **2020**, *521*, 146375.

12. Vaz, J.M.; Taketa, T.B.; Hernandez-Montelongo, J.; Chevallier, P.; Cotta, M.A.; Mantovani, D.; Beppu, M.M. Antibacterial properties of chitosan-based coatings are affected by spacer-length and molecular weight. *Appl. Surf. Sci.* **2018**, *445*, 478–487.

13. Thukkaram, M.; Cools, P.; Nikiforov, A.; Rigole, P.; Coenye, T.; Van Der Voort, P.; Du Laing, G.; Vercruysse, C.; Declercq, H.; Morent, R.; et al. Antibacterial activity of a porous silver doped TiO2 coating on titanium substrates synthesized by plasma electrolytic oxidation. *Appl. Surf. Sci.* **2020**, *500*, 144235.

14. Manakhov, A.; Permyakova, E.S.; Ershov, S.; Sheveyko, A.; Kovalskii, A.; Polčák, J.; Zhitnyak, I.Y.; Gloushankova, N.A.; Zajíčková, L.; Shtansky, D. V. Bioactive TiCaPCON-coated PCL nanofibers as a promising material for bone tissue engineering. *Appl. Surf. Sci.* **2019**, *479*, 796–802.

15. Sukhorukova, I. V.; Sheveyko, A.N.; Kiryukhantsev-Korneev, P. V.; Levashov, E.A.; Shtansky, D. V. *In vitro* bioactivity study of TiCaPCO(N) and Ag-doped TiCaPCO(N) films in simulated body fluid. *J. Biomed. Mater. Res. Part B Appl. Biomater.* **2015**, n/a-n/a.

16. Shtansky, D. V.; Batenina, I. V.; Kiryukhantsev-Korneev, P. V.; Sheveyko, a. N.; Kuptsov, K. a.; Zhitnyak, I.Y.; Anisimova, N.Y.; Gloushankova, N. a. Ag- and Cu-doped multifunctional bioactive nanostructured TiCaPCON films. *Appl. Surf. Sci.* **2013**, *285*, 331–343.

17. Sukhorukova, I. V.; Sheveyko, a. N.; Kiryukhantsev-Korneev, P. V.; Anisimova, N.Y.; Gloushankova, N. a.; Zhitnyak, I.Y.; Benesova, J.; Amler, E.; Shtansky, D. V. Two approaches to form antibacterial surface: Doping with bactericidal element and drug loading. *Appl. Surf. Sci.* **2015**, *330*, 339–350.

18. Hu, R.; Li, G.; Jiang, Y.; Zhang, Y.; Zou, J.-J.; Wang, L.; Zhang, X. Silver–Zwitterion Organic–Inorganic Nanocomposite with Antimicrobial and Antiadhesive Capabilities. *Langmuir* **2013**, *29*, 3773–3779.

19. Manakhov, A.; Kiryukhantsev-Korneev, P.; Michlíček, M.; Permyakova, E.; Dvořáková, E.; Polčák, J.; Popov, Z.; Visotin, M.; Shtansky, D. V. Grafting of carboxyl groups using CO2/C2H4/Ar pulsed plasma: Theoretical modeling and XPS derivatization. *Appl. Surf. Sci.* **2018**, *435*, 1220–1227.

20. Cools, P.; Declercq, H.; De Geyter, N.; Morent, R. A stability study of plasma polymerized acrylic acid films. *Appl. Surf. Sci.* **2017**.

21. Shtansky, D. V.; Sheveyko, A.N.; Sorokin, D.I.; Lev, L.C.; Mavrin, B.N.; Kiryukhantsev-Korneev, P. V. Structure and properties of multi-component and multilayer TiCrBN/WSex coatings deposited by sputtering of TiCrB and WSe2 targets. *Surf. Coatings Technol.* **2008**, *202*, 5953–5961.

22. Sukhorukova, I.V.; Sheveyko, A.N.; Manakhov, A.; Zhitnyak, I.Y.; Gloushankova, N.A.; Denisenko, E.A.; Filippovich, S.Y.; Ignatov, S.G.; Shtansky, D.V. Synergistic and long-lasting antibacterial effect of antibiotic-loaded TiCaPCON-Ag films against pathogenic bacteria and fungi. *Mater. Sci. Eng. C* **2018**, *90*, 289–299.

23. Manakhov, A.; Michlíček, M.; Felten, A.; Pireaux, J.-J.; Nečas, D.; Zajíčková, L. XPS depth profiling of derivatized amine and anhydride plasma polymers: Evidence of limitations of the derivatization approach. *Appl. Surf. Sci.* **2017**, *394*, 578–585.

24. Degoutin, S.; Jimenez, M.; Chai, F.; Pinalie, T.; Bellayer, S.; Vandenbossche, M.; Neut, C.; Blanchemain, N.; Martel, B. Simultaneous immobilization of heparin and gentamicin on polypropylene textiles: A dual therapeutic activity. *J. Biomed. Mater. Res. - Part A* **2014**, *102*, 3846–3854.

25. Croes, S.; Stobberingh, E.E.; Stevens, K.N.J.; Knetsch, M.L.W.; Koole, L.H. Antimicrobial and anti-thrombogenic features combined in hydrophilic surface coatings for skin-penetrating catheters. Synergy of co-embedded silver particles and heparin. *ACS Appl. Mater. Interfaces* **2011**, *3*, 2543–2550.

26. Körner, E.; Aguirre, M.H.; Fortunato, G.; Ritter, A.; Rühe, J.; Hegemann, D. Formation and distribution of silver nanoparticles in a functional plasma polymer matrix and related Ag+ release properties. *Plasma Process. Polym.* **2010**, *7*, 619–625.

27. Suvannapruk, W.; Thammarakcharoen, F.; Phanpiriya, P.; Suwanprateeb, J. Development of antibiotics impregnated nanosized silver phosphate-doped hydroxyapatite bone graft. *J. Nanomater.* **2013**, *2013*.

27. Lassila, T.; Hokkanen, J.; Aatsinki, S.-M.; Mattila, S.; Turpeinen, M.; Tolonen, A. Toxicity of carboxylic acid-containing drugs: The role of acyl migration and CoA conjugation investigated, *Chem. Res. Toxicol.* **2015**, *28*, 2292-2303.

28. Suvannapruk, W.; Thammarakcharoen, F.; Phanpiriya, P.; Suwanprateeb, J. Development of antibiotics impregnated nanosized silver phosphate-doped hydroxyapatite bone graft. *J.*

Nanomater. **2013**, *2013,* 542584.

29. Park, H.-J.; Kim, J.Y.; Kim, J.; Lee, J.-H.; Hahn, J.-S.; Gu, M.B.; Yoon, J. Silver-ion-mediated reactive oxygen species generation affecting bactericidal activity, *Water Res.* **2009**, *43*, 1027-1032.
30. Tolan. D.; Gandin V.; Morrison, L.; El-Nahas, A.; Marzano, C.; Montagner, D.; Erxleben, A. Oxidative stress induced by Pt(IV) pro-drugs based on the cisplatin scaffold and indole carboxylic acids in axial position, *Sci. Rep.* **2016**, *6*, 29367.
31. Fu, P.P.; Xia, Q.; Xwang, H.-M.; Ray, P.C.; Yu, H. Mechanisms of nanoctoxicity: Generation of reactive oxygen species, *J. Food Drug Anal.* **2014**, *22*, 64-75.
32. Haase, A.; Rott, S.; Mantion, A.; Graf, P.; Plendi, J.; Thünemann, A.F.; Meier, W.P.; Taubert, A.; Luch, A.; Reiser, G. Effects of silver nanoparticles on primary mixed neural cell cultures: uptake, oxidative stress and acute calcium responses. *Toxicol. Sci.* **2012**, *126*, 457–468.
33. He, D.; Dorantes-Aranda, J.J.; Waite, T.D. Silver nanoparticle algae interactions: oxidative dissolution, reactive oxygen species generation and synergistic toxic effects. *Environ. Sci. Technol.* **2012**, *46*, 8731–8738.
34. Awasthi, K.K.; Awasthi, A.; Kumar, N.; Awasthi, K.; Jhon, P.J. Silver nanoparticle induced cytotoxicity, oxidative stress, and DNA damage in CHO cells. *J. Nanopart. Res.* **2013**, *15*, 1898.
35. Cheng, X.; Zhang, W.; Yinqlu, J.; Menq, J.; Wu, X.; Xu, H. Revealing silver cytotoxicity using Au nanorods/Ag shell nanostructures: disrupting cell membrane and causing apoptosis through oxidative damage. *RSC Adv.* **2013**, *3*, 2296–2305